# Supplementary material to "Mechanism of Radiation Damage Reduction in Equiatomic Multicomponent Single Phase Alloys"

F. Granberg
*Department of Physics, Post-office box 43, FIN-00014 University of Helsinki, Finland*

K. Nordlund
*Department of Physics, Post-office box 43, FIN-00014 University of Helsinki, Finland**

Mohammad W. Ullah
*Department of Physics, Post-office box 43, FIN-00014 University of Helsinki, Finland and*
*Materials Science and Technology Division, Oak Ridge National Laboratory, Oak Ridge, Tennessee 37831, USA*

K. Jin
*Materials Science and Technology Division, Oak Ridge National Laboratory, Oak Ridge, Tennessee 37831, USA*

C. Lu
*Department of Nuclear Engineering and Radiological Sciences,*
*University of Michigan, Ann Arbor, Michigan 48109-2104, USA*

H. Bei
*Materials Science and Technology Division, Oak Ridge National Laboratory, Oak Ridge, Tennessee 37831, USA*

L. M. Wang
*Department of Nuclear Engineering and Radiological Sciences,*
*University of Michigan, Ann Arbor, Michigan 48109-2104, USA*

F. Djurabekova
*Helsinki Institute of Physics, Post-office box 43, FIN-00014 University of Helsinki, Finland and*
*Department of Physics, Post-office box 43, FIN-00014 University of Helsinki, Finland*

W. J. Weber
*Materials Science and Technology Division, Oak Ridge National Laboratory, Oak Ridge, Tennessee 37831, USA and*
*Department of Materials Science and Engineering,*
*University of Tennessee, Knoxville, Tennessee 37996, USA*

Y. Zhang
*Materials Science and Technology Division, Oak Ridge National Laboratory, Oak Ridge, Tennessee 37831, USA*†

(Dated: March 23, 2016)

## SUPPLEMENTARY MOVIES

The supplementary material includes the two movie files

Ni-5kev-1500-recoils.mov

and

NiFe-5kev-1500-recoils.mov

These quicktime movies illustrate the buildup of damage in Ni and NiFe (see main Letter). The movies show a 2D projection of all atom positions in a cubic simulation cell that is 108 Å in each dimension. Each dot illustrates the position of an atom, with blue dots representing Ni and red dots Fe. Each frame shows the final atom positions after one irradiation cascade event. The irradiation dose is given in units of displacements-per-atom (dpa).

Since the cells are crystalline, atoms in the same perfect crystal row are all plotted on top of each other, and hence only the atoms at the top are visible. Atoms in interstitial defects and stacking faults are, however, visible at any depth since they are outside the perfect crystal rows.

The movies show how, after the first few irradiation events, small stacking faults (bounded by partial dislocation loops) form in the cells. On increasing dose, they grow when additional cascades form damage near them,

and part of this damage is absorbed by the preexisting defects. The dislocation structures are also made mobile by the lattice heating and distortion caused by additional irradiation, evident from the rapid motion of defective regions. At the highest doses, the damage level has saturated (compare Fig. 4 in main Letter).

Comparison of the Ni and NiFe movies show that the defect structures in NiFe tend to be smaller than those in Ni (cf. detailed discussion in main Letter).

## DETAILS ON METHODS

**Synthesis of equiatomic alloys**.

Polycrystalline ingots of Ni metal and Ni-based equiatomic alloys were prepared using high-purity elemental metals (> 99.9% purity) by arc melting and drop casting into cylindrical copper molds. The phase stability and the formation of single phases were carefully examined and confirmed using X-ray diffraction and microstructure characterization techniques [1]. The phase diagram for the investigated alloys, showing their phase stability, can be found for Ni and NiFe in Ref. 2 and the theoretical prediction of the phase stability of NiCoCr in Ref. 3. Face-centered cubic crystal Ni and alloys were grown in an optical floating zone furnace from the polycrystalline drop-cast ingots under an Ar atmosphere [4]. The quality and orientation of all crystals were inspected using backscatter Laue diffraction, re-oriented and cut normal to the <100> directions. Disks with thickness of $\sim$ 1 mm were electrochemically polished to remove the damage layers of the machining in order to produce damage-free surfaces, essential for ion channeling measurements.

**Ion irradiation.**

Irradiation response at room temperature of Ni, NiFe and NiCoCr were investigated with 3 MeV Au ions to fluences of $2 \times 10^{13}$, $5 \times 10^{13}$ and $1 \times 10^{14}$ cm$^{-2}$ and 1.5 MeV Ni ions to $6 \times 10^{13}$, $1 \times 10^{14}$ and $2 \times 10^{14}$ cm$^{-2}$. Raster beam was used to ensure a homogeneous irradiation. The irradiation-induced damage peak was located at $\sim$ 155 nm and 370 nm for the Au and Ni cases, respectively. These energies were chosen to produce damage within a few hundreds of nanometers from the sample surface, where the damaged region can be readily characterized by microstructural analysis and ion channeling measurements with good depth resolution, but deep enough to avoid complication from surface effects. Predictions of local dose in displacements per atom (dpa) [5] and ion stopping range in Ni were estimated using the Stopping and Range of Ions in Matter (SRIM) code [6] under option of quick calculation of damage with a displacement threshold energy of 40 eV. The measured density of 8.908 g cm$^{-3}$ is used in the SRIM calculation for pure Ni.

**Rutherford backscattering and ion channeling analysis.**

Rutherford backscattering spectrometry technique along major channel directions is used to verify the crystal quality and also to determine lattice distortion. A parallel 3.5 MeV He$^+$ beam that was well aligned along the <001> crystal direction was employed in the measurements. Following the ion energy deposition by either energetic Au ions or Ni ions, in-situ channeling measurements were subsequently carried out with a Si detector located at a scattering angle of 155° relative to the incoming He beam to record the increase of the backscattering yield due to irradiation-induced damage.

**Microstructural characterization.**

The cross-sectional TEM samples were prepared using focused ion beam (FIB) lift-out techniques utilizing the FEI Helios 650 Nanolab Dualbeam workstation. FIB-induced damage and sample thinning were performed by Ga$^+$ beam initially with energy of 30 keV and a current of 2.5 nA to 30 pA at an incident angle of $\pm$1.5° and sequentially down to 5 keV at the angle of $\pm$7° for 5 min. A flash polishing was conducted to remove residual damage from sample preparation. Bright field imaging of the same samples was done in a JEM 3011 TEM operating at 300 kV. Images were taken at an exposure time of 2 seconds.

**Simulations.**

The collision cascades in metals were simulated by means of molecular dynamics [7, 8] using the fully parallel PARCAS code developed within the group in Finland and extensively used for studies of cascades previously [9, 10]. We used two different potentials to describe the interatomic interactions in NiFe and NiCoCr alloys to verify that there is no significant dependence of the results on the choice of the interatomic potential. To describe the Ni-Co-Cr system, we combined the multi-elemental potentials by Zhou *et al.* [11] for Ni-Co with the Cr potential in the same formalism developed by Lin *et al.* [12]. To describe the interactions between the different elements in this system, we used the mixing scheme proposed in [11] between all the elements Ni-Co-Cr. For Fe-Ni, we used both the Fe-Ni potential formed in the same Zhou *et al.* set of potentials [11], and the completely independently developed pair-specific Fe-Ni potential by Bonny *et al.* [13]. Neither of the used potentials ex-

plicitly accounts for magnetism. Nevertheless it is implicitely taken into account, for instance, in the fitting of the cohesive energy. This remark is important with respect to results on damage buildup in FeNi, which is a magnetic material. However, previous simulation results on damage production in Fe with an explicit magnetic potential showed no significant difference compared to non-magnetic potentials. [14, 15] This justifies the use of potentials, where the magnetism is only implicitly accounted for. Both the Fe-Ni potentials were found to give similar results with respect to the damage production, showing that the results are not specific to a certain interatomic potential.

All three elemental compositions, Ni, NiFe and NiCoCr were simulated up to the dose $\sim 0.57$ dpa by running 1500 consecutive 5 keV recoils. Each set of the 1500 recoils was repeated three different times for each system using different seed numbers in the random number generator and different initial random cells, to show that the obtained results are not due to stochastic anomalities.

We dealt with the high energy effects associated with collision cascades by employing well established simulation methods for irradiation effects, namely an adaptive time step algorithm [16], electronic stopping power [17] and the ZBL repulsive potential [6] smoothly joined to the equilibrium potentials to describe the short distance interactions [9].

We used simulation cells comprising about 110 000 atoms to ensure that the heat spikes induced by the 5 keV recoils were fully developed within the cell, and that the periodic boundary conditions (applied at the cell sides in all dimensions) did not affect the final results. The simulation cell is too small for the largest defect structures seen in experiments (can be larger than 10 nm) to be represented, but a separate simulation setup, in FeCr, on a three times larger system showed that the damage level saturates at similar doses and defect levels, indicating that the key results are not sensitive to the system size.

During the cascade simulations, we controlled the temperature only at the sides of the simulation cell by applying Berendsen temperature control [18] on the border atoms. After about 25 ps (of the simulated 30 ps), no visible change in the damage structure was observed any more and the entire cell had cooled down to the ambient temperature (300 K). This will, as mentioned in the Letter, yield a much higher dose rate than that used in the experiments. However, the previous studies with similar approaches to simulate the damage buildup in semiconductors have shown a good agreement with experiments, although there was a similarly large difference in the dose rates [19, 20]. We ensured the homogeneous irradiation of the simulation cell by shifting the entire cell prior to the subsequent recoil event by a vector of random length (between zero and the cell size) and in a random direction. After the shift, atoms that were outside the cell boundaries were returned inside via the periodic cell boundaries. We monitored the development of stress in the simulations, and found no significant buildup of stress during the prolonged irradiation. A separate simulation was performed where a step of pressure relaxation to 0 kbar between the recoil events was added. This simulation gave identical results within statistical fluctuations to those without the extra step of pressure control.

Defects were analyzed with the Wigner-Seitz cell method [9] as well as with the program OVITO [21] and an adaptive common neighbor analysis implemented in the program.

### Comparison with ferritic alloys

Currently a leading candidate class of materials for high radiation environments are ferritic steels based on about 10% Cr in a body-centered cubic (Fe) matrix [22, 23], which have been shown to exhibit good radiation resistance, likely due to the Cr slowing down dislocation loop migration [24, 25]. Hence, even though the Fe-Cr crystal structure is different to the currently studied face-centered cubic systems, it is of some interest to qualitatively compare the current results to those in Fe-10%Cr alloys. Hence we ran a set of similar cumulative 5 keV simulations for this Fe-Cr system modelled with the Olsson *et al.* potential [26]. The results of the comparison, Fig. 1, show that reduction in irradiation damage is superior for the equiatomic alloys compared to iron and the Fe-Cr alloy. We emphasize that the numerical values should not be compared directly to each other, due to differences in the crystal structure, but the relative change difference between the pair of element vs. alloys gives a first indication that the damage reductions obtained in equiatomic alloys may be quite comparable, or even better, than those in long-developed Fe-Cr alloys. However, as for the final Fe-Cr based steels which have undergone decades of development, clearly more work will be needed also on testing and optimizing alloying element concentrations and microstructure for equiatomic alloys, before they are ready for use as engineering materials.

## SOURCE CODE AND INPUTS

To enable reproduction of the results, the Supplementary material also includes the complete source code of the software used to carry out the simulations 'parcas' [27]. The code, its documentation, and sample inputs for

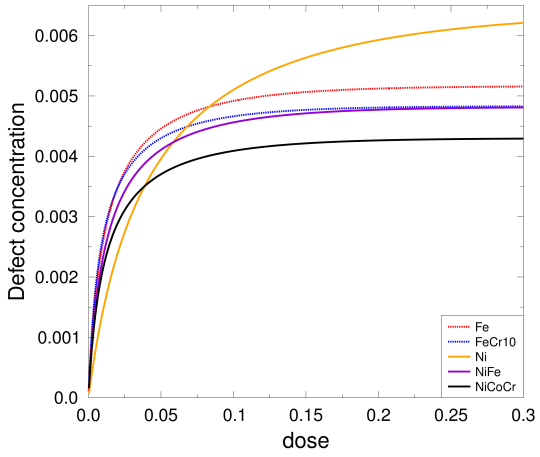


FIG. 1. Comparison of the results obtained for the equiatomic alloys compared with Fe and $Fe_{0.9}Cr_{0.1}$

Ni, NiFe and NiCoCr are provided as a `tar` archive package compressed in the `gzip` format. The package can be unpacked using the Linux/Unix command line command

```
tar xvfz parcas_source_code_inputs_package.tar.gz
```

The code can be compiled and run on any Linux/Unix distribution that carries, in addition to the standard system environment, an MPI Fortran compiler, following normal practises of Linux software compilation and execution. The file

```
README.INSTALL
```

provided in the main directory created by the unpacking contains installation and running instructions.

* kai.nordlund@helsinki.fi; Corresponding author
† Zhangy1@ornl.gov; Corresponding author

[1] Z. Wu, H. Bei, F. Otto, G. M. Pharra, and E. P. George, Intermetallics **46**, 131 (2014).
[2] B. Predel, *Phase Equilibria, Crystallographic and Thermodynamic Data of Binary Alloys*, edited by O. Madelung, Landolt-Börnstein, New Series III, Vol. IV/5 (Springer, Berlin, 1992).
[3] M. C. Troparevsky, J. R. Morris, P. R. C. Kent, A. R. Lupini, and G. M. Stocks, Phys. Rev. X **5**, 011041 (2015).
[4] H. Bei and E. George, Acta Materialia **53**, 69 (2005).
[5] R. Stoller, M. B. Toloczko, G. S. Was, A. G. Certain, S. Dwaraknath, and F. Garner, Nucl. Instr. Meth. Phys. Res. B **310**, 75 (2013).
[6] J. F. Ziegler, J. P. Biersack, and U. Littmark, *The Stopping and Range of Ions in Matter* (Pergamon, New York, 1985).
[7] M. P. Allen and D. J. Tildesley, *Computer Simulation of Liquids* (Oxford University Press, Oxford, England, 1989).
[8] M. Ghaly, K. Nordlund, and R. S. Averback, Phil. Mag. A **79**, 795 (1999).
[9] K. Nordlund, M. Ghaly, R. S. Averback, M. Caturla, T. Diaz de la Rubia, and J. Tarus, Phys. Rev. B **57**, 7556 (1998).
[10] K. Nordlund, J. Keinonen, M. Ghaly, and R. S. Averback, Nature **398**, 49 (1999).
[11] X. W. Zhou, R. A. Johnson, and H. N. G. Wadley, Phys. Rev. B **69**, 144113 (2004).
[12] Z. Lin, R. A. Johnson, and L. V. Zhigilei, Phys. Rev. B **77** (2008).
[13] G. Bonny, N. Castin, and D. Terentyev, Modelling Simul. Mater. Sci. Eng. **21**, 085004 (2013).
[14] C. Björkas and K. Nordlund, Nucl. Instr. Meth. Phys. Res. B **259**, 853 (2007).
[15] L. Malerba, M. C. Marinica, N. Anento, C. Björkas, H. Nguyen, C. Domain, F. Djurabekova, P. Olsson, K. Nordlund, A. Serra, D. Terentyev, F. Willaime, and C. Becquart, J. Nucl. Mater. **406**, 19 (2010).
[16] K. Nordlund, Comput. Mater. Sci. **3**, 448 (1995).
[17] J. F. Ziegler, SRIM-2013 software package, available online at *http://www.srim.org*.
[18] H. J. C. Berendsen, J. P. M. Postma, W. F. van Gunsteren, A. DiNola, and J. R. Haak, J. Chem. Phys. **81**, 3684 (1984).
[19] J. Nord, K. Nordlund, and J. Keinonen, Nucl. Instr. Meth. Phys. Res. B **193**, 294 (2002).
[20] M. Backman, F. Djurabekova, O. H. Pakarinen, K. Nordlund, L. L. Araujo, and M. C. Ridgway, Phys. Rev. B **80**, 144109 (2009).
[21] A. Stukowski, Modelling and Simulation in Materials Science and Engineering **20**, 045201 (2012).
[22] K. Murty and I. Charit, J. Nucl. Mater. **383**, 189 (2008).
[23] S. J. Zinkle and J. T. Busby, Materials Today **12**, 12 (2009).
[24] D. Terentyev, M. Klimenkov, and L. Malerba, J. Nucl. Mater. **393**, 30 (2009).
[25] L. Malerba, G. Bonny, D. Terentyev, E. E. Zhurkin, M. Hou, K. Vörtler, and K. Nordlund, J. Nucl. Mater. **442**, 486 (2013).
[26] P. Olsson, J. Wallenius, C. Domain, K. Nordlund, and L. Malerba, Phys. Rev. B **72**, 214119 (2005), see also Erratum, Phys. Rev. B 74, 229906 (2006).
[27] K. Nordlund, (2010), PARCAS computer code. The main principles of the molecular dynamics algorithms are presented in [8, 9]. The adaptive time step and electronic stopping algorithms are the same as in [16].